ATMOSPHERIC SCIENCE

Climate models generally underrepresent the warming by Central Africa biomass-burning aerosols over the Southeast Atlantic

Marc Mallet[1]*, Pierre Nabat[1], Ben Johnson[2], Martine Michou[1], Jim M. Haywood[2,3], Cheng Chen[4,5], Oleg Dubovik[5]

The radiative budget, cloud properties, and precipitation over tropical Africa are influenced by solar absorption by biomass-burning aerosols (BBA) from Central Africa. Recent field campaigns, reinforced by new remote-sensing and aerosol climatology datasets, have highlighted the absorbing nature of the elevated BBA layers over the South-East Atlantic (SEA), indicating that the absorption could be stronger than previously thought. We show that most of the latest generation of general circulation models (GCMs) from the sixth phase of the Coupled Model Intercomparison Project 6 (CMIP6) underestimates the absorption of BBA over the SEA. This underlines why many (~75%) CMIP6 models do not fully capture the intense positive (warming) direct radiative forcing at the top of the atmosphere observed over this region. In addition, underestimating the magnitude of the BBA-induced solar heating could lead to misrepresentations of the low-level cloud responses and fast precipitation feedbacks that are induced by BBA in tropical regions.

INTRODUCTION

Recently, the South-East Atlantic (SEA) region has been the center of focused international attention through the deployment of large-scale measurement campaigns [Layered Atlantic Smoke Interactions with Clouds (LASIC) (*1*), Dynamics-Aerosol-Chemistry-Cloud Interactions in West Africa (DACCIWA) (*2*), ObseRvations of Aerosols above CLouds and their intEractionS (ORACLES) (*3*), CLoud-Aerosol-Radiation interaction and forcing (CLARIFY-2017) (*4*), and Aerosols, Radiation and Clouds in Southern Africa (AEROCLO-sA) (*5*)] aiming to understand the role of biomass-burning aerosols (BBA) emitted over Central Africa (mainly in Congo, Angola, and Zambia) on the radiative balance and climate of this region. A unique feature of these BBA layers is their ability to strongly absorb solar radiation (*1*), thereby affecting the radiative balance, cloudiness, and precipitation in different ways when compared to nonabsorbing particles such as sulfate and sea salt that more typically dominate aerosol concentrations in marine environments. The particles are primarily composed of organic matter, black carbon, and inorganic species such as potassium, chloride, sulfate, and nitrate (*6*). By overlying the quasi-permanent stratocumulus clouds over the SEA, these absorbing smoke aerosols that have been transported over the ocean are known to produce an intense (warming) positive direct effect [monthly mean between ~0 up to +8 W m $^{-2}$ (*7*–*9*)] at the top of the atmosphere. This is a unique region in terms of the sign and magnitude of the aerosol direct radiative effect, making it a prominent feature of aerosol forcing at the global scale. The pattern occurs every year during the biomass-burning season from June to October (*7*). Quantifying the warming induced by the BBA over the SEA is very important for the radiative balance and climatic feedbacks in the region (*10*), but it still remains particularly difficult to represent with fidelity in general circulation models (GCMs) as it relies on accurately representing the smoke vertical structure, spatial distribution, and vertical structure of stratocumulus clouds and the BBA optical properties [i.e., single-scattering albedo (SSA), spectral aerosol optical depth (AOD), and asymmetry parameter] (*11*). Currently, this warming effect is not well constrained in GCMs (*4*, *12*).

In addition, absorbing BBA have important secondary impacts on low-cloud Sc properties over the SEA related to the effect of radiative heating on the relative humidity and temperature profiles via what is known as semidirect effect (*13*). Although important uncertainties still remain on how the semidirect forcing of absorbing aerosols affects low stratocumulus clouds (*14*), a consensus is emerging for the SEA region. Several studies based on large eddy simulations (*15*, *16*), global or regional climate models (*10*, *17*, *18*), and satellite observations (*19*, *20*) all indicate that BBA generally increases low-level cloud cover, although other cloud microphysical effects also operate (*21*). Changes in low clouds are known to be one of the strongest agents of radiative feedback in the climate system due to their high albedo (*22*). In addition to these effects on radiation and clouds, the substantial absorption by BBA can also affect atmospheric stability, circulation, and precipitation and BBA have the potential to inhibit convection (increasing the static stability) (*23*) with strong implications on the hydrological cycle (*10*, *24*). Some studies (*25*, *26*) have recently underlined the important impacts of BBA radiative effects over the Western African monsoon region where aerosol forcing can decrease precipitation, especially over southern West Africa, which has one of the fastest-growing populations worldwide.

Among the different results obtained under the recent international projects, one common finding is that the absorption by BBA appears to be higher than previously thought (*1*, *6*, *27*, *28*) with an SSA (the ratio of aerosol scattering to extinction efficiency) as low as ~0.80 (at 550 nm). A particular advance in these recent estimates is the deployment of highly accurate cavity ring down measurements

[1]CNRM, Université de Toulouse, Météo-France, CNRS, Toulouse, France. [2]Met Office, Exeter EX1 3PB, UK. [3]College of Engineering, Mathematics and Physical Science, University of Exeter, Exeter EX4 4QE, UK. [4]GRASP SAS, 59000 Lille, France. [5]Université de Lille, CNRS, UMR 8518, LOA–Laboratoire d'Optique Atmosphérique, 59000 Lille, France.
*Corresponding author. Email: marc.mallet@meteo.fr

of aerosol extinction and photo-acoustic measurements of aerosol absorption on aircraft (*6*, *29*), allowing the SSA to be derived with high accuracy during those experimental campaigns. These observations raise the question whether the strong absorption is adequately captured in global models, including the latest Coupled Model Intercomparison Project 6 (CMIP6) configurations, and, consequently, if they accurately represent the various impacts of BBA on climate in the SEA. To address this question, we develop an approach using polarization and anisotropy of reflectances for atmospheric sciences coupled with observations from a lidar (PARASOL) satellite observations derived using a recently described method (*30*), AErosol RObotic NETwork (AERONET) surface remote-sensing, recent in situ (surface and aircraft) observations and the recently developed MACv2 aerosol (monthly optical properties derived from a combination of observations and model outputs, see the "Observation data" section) dataset (*31*) to evaluate the latest generation of CMIP6 models. We show that these models do not fully capture the strong BBA solar absorption over the SEA. These results are contrary to those obtained (*32*) from a similar assessment based on the comparison of eight global models with aircraft observations from a broader selection of BBA regions that included Africa, South America, North America, northern Asia, and southeastern Asia. These differences in results may stem from the fact that the study areas are not exactly the same, as well as the number and version of the participating models and differences in the treatment of biomass burning emissions, optical properties, and mixing state. Furthermore, the Africa domain used in (*32*) is not necessarily representative of smoke plume transported over SEA.

This bias in absorption by BBA, together with the difficulty of CMIP6 models to reproduce the large low cloud fraction (CF) over stratocumulus regions (*33*), explains why many (~75%) CMIP6 models are not able to reproduce the strong positive (warming) effect at the top of the atmosphere over the SEA. We demonstrate that, in their present configurations, the key radiative feedback (BBA-induced heating) controlling the semidirect effect of smoke aerosols on low-level clouds (*15*) is likely to be too weak in some global models. We argue that the underrepresentation of BBA-induced heating in GCMs would lead to insufficient increases in low-level stratocumulus clouds, which are known to be extremely important for the radiation/climatic balance (*22*). Our findings make it difficult to have confidence in other fast responses linked to BBA solar absorption, such as precipitation feedbacks (*34*) over the tropics during the biomass-burning season including the drying effect of BBA recently highlighted by (*25*, *26*) over the densely populated southern West African region.

RESULTS

Absorbing properties of smoke aerosols over the tropical Africa

We evaluate the solar absorption of smoke aerosols in the SEA region simulated by the CMIP6 models by comparing the mean SSA obtained during the July-August-September (JAS) season (period 2003–2014) against that derived by PARASOL/Generalized Retrieval of Aerosol and Surface Properties (GRASP) (*30*) (see the "Evaluation/observation data" section) and MACv2 data (Fig. 1). We also compared the modeled SSA with that retrieved from AERONET inversions (*35*, *36*) (see the "Evaluation/observation data" section) at three main stations, such as Lubango, Mongu, and Ascension Island. These comparisons show a large range of outcomes from the models. Some models (AWI-ESM-1-1-LR, CESM2, CESM-WACCM, E3SM, GFDL, or MRI-ESM) were able to represent the SSA over the continent with small and relatively acceptable biases [between ±0.04, corresponding to AERONET uncertainties (*36*)] compared to AERONET (Fig. 1). A few models (including versions of HadGEM3, CanESM, and some versions of GISS-E2) had a negative bias in SSA, but a larger proportion, some 11 of the CMIP6 models, significantly overestimated SSA (i.e., underestimate absorption) over the continental part of tropical Africa. The most significant high biases in SSA were from the MIROC-ES2L, INM-CM4-8, ISPL-LR, INM-CM5-0, NorESM2-LM, and CNRM-CM6 models. This high spread in modeled SSA is further highlighted by the comparisons at the two continental (Mongu and Lubango) AERONET stations (Fig. 2A). The results here also show that the well-defined seasonal cycle of SSA that is seen in AERONET observations during the biomass-burning season (*37*) is not fully reproduced by the CMIP6 models. At both Lubango and Mongu AERONET stations, the average for the CMIP6 global models does not quite reach as low as the observed AERONET SSA (~0.83) during July-August.

The models have a stronger tendency to overestimate SSA at Ascension Island (Fig. 2A) and most appear progressively too scattering compared to PARASOL/GRASP and MACv2 in downwind regions further from source (Fig. 1). Furthermore, the seasonal cycle of SSA at Ascension Island, as derived from AERONET, MACv2, and PARASOL/GRASP, is not reproduced by models, which are characterized by rather constant SSA (~0.95) throughout the year. These findings could indicate that models are not reproducing the full westward extent of highly absorbing aged smoke aerosols observed over the tropical SEA.

A longitudinal transect has been defined (Fig. 1, MACv2) that passes through the three AERONET stations and traverses the stratocumulus clouds region and the overlying smoke. Along this track, there is a significant increase in the SSA bias in CMIP6 models compared to PARASOL/GRASP and MACv2, as highlighted by the contrast between BBA sources (right) and the outflow (left) (Fig. 2B). We find that CMIP6 models diverge further from observations toward higher SSA values westward of 6°E compared to the satellite-derived and MACv2 datasets that present a remarkably stable SSA (~0.88) between 10°E and 14°W and agree with the AERONET SSA at Ascension Island. Further evidence of this discrepancy comes from the surface [LASIC (*11*)] and aircraft [ORACLES-2016 (*27*) and CLARIFY-2017 (*6*)] measurements recently obtained over the SEA that strongly reinforce the presence of extremely absorbing smoke aerosols with low SSA (between ~0.80 and 0.86, at 550 nm) (Fig. 2B) for aged smoke (typically more than 2 days after emissions), which are not fully reproduced in the latest versions of CMIP6 models.

Because of the large above-cloud AOD of smoke in this region (*3*), the overestimation of smoke SSA may have large implications for a range of climate-relevant effects, including the direct radiative effect exerted at the top of the atmosphere, especially over the stratocumulus region, the heating rate at the altitude of transport [~700 hPa; (*38*)], the semidirect forcing on low-level clouds and the fast responses in precipitation over tropical Africa (*34*). All of these possible implications are discussed below. To help the analysis, different groups of CMIP6 models have been categorized on the basis of their bias in SSA and CF over the SEA [with SSA compared

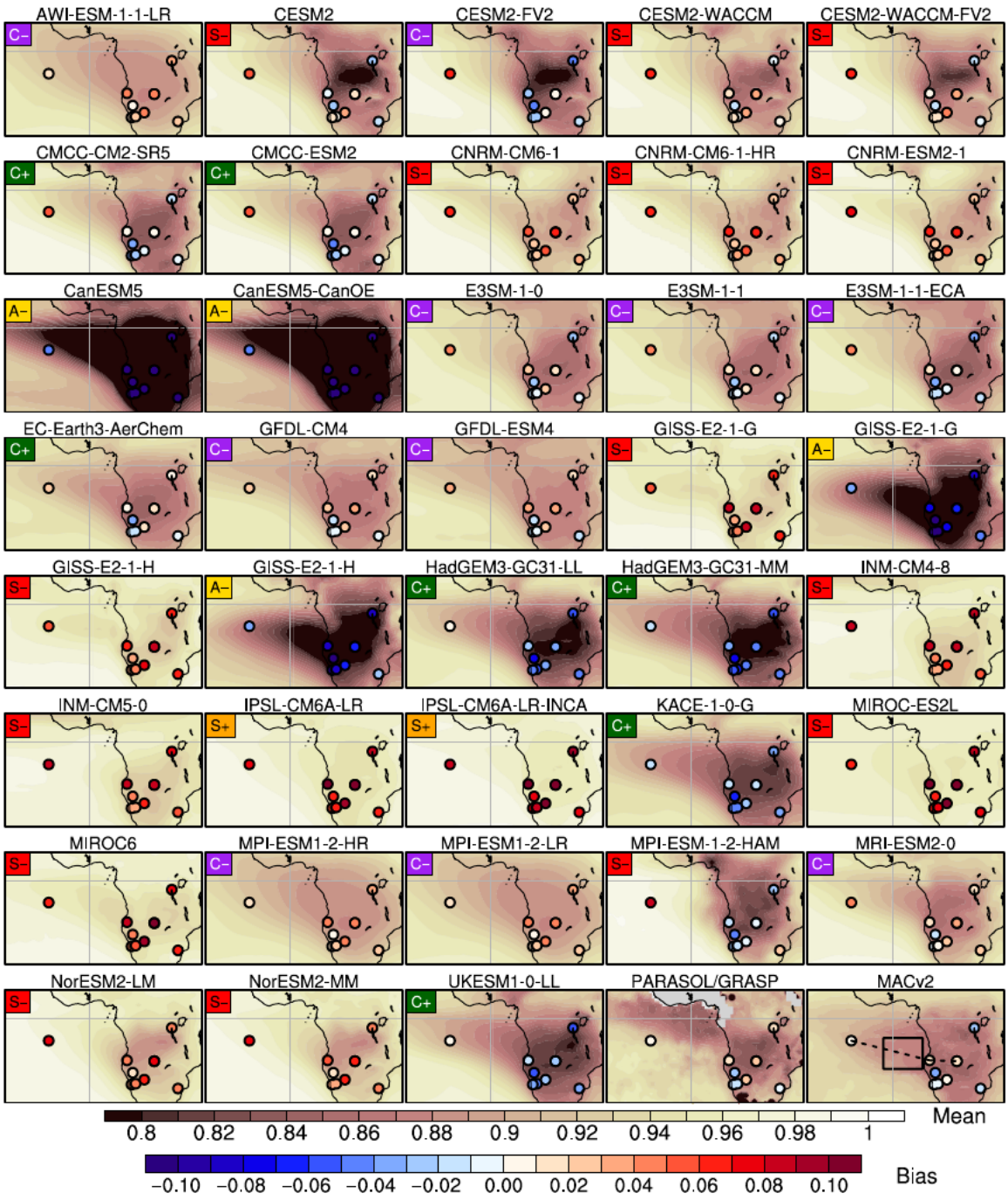

Fig. 1. Aerosol SSA over tropical Africa. Averaged JAS SSA (at 550 nm) for each of the CMIP6 models, as well as PARASOL/GRASP and MACv2 data. The bias against AERONET stations is represented with colored (blue to red) points. All models are classified depending on their ability to reproduce SSA over the SEA (C for correct, S for too scattering, and A for too absorbing) and CF [noted (+) for bias in CF ≤ 25% or (–) for CF bias >25% compared to CALIOP datasets; see Materials and Methods and figs. S1 and S3]. The box (3°W to 11°E 7°S to 18°S) is used to quantify the CF and SSA biases (see Materials and Method). The MACv2 plot (bottom right) illustrates the transect used for the analysis in Fig. 2.

against MACv2 and CF against Cloud Aerosol Lidar with Orthogonal Polarization (CALIOP); see Materials and Methods]. For the SSA, models are either denoted as having a positive bias (group S, i.e., too scattering), a negative bias (group A, i.e., too absorbing), or a near-zero bias (group C, correct). For CF, models are gathered in two groups: + for a relatively small bias and − for a large negative bias (insufficient low clouds). By merging the two variables, five groups (table S1) of models are analyzed: C+ (for correct SSA and good CF), C− (correct SSA/poor CF), S+ (overestimated SSA/good CF), S− (overestimated SSA/poor CF), and A− (underestimated SSA/poor CF).

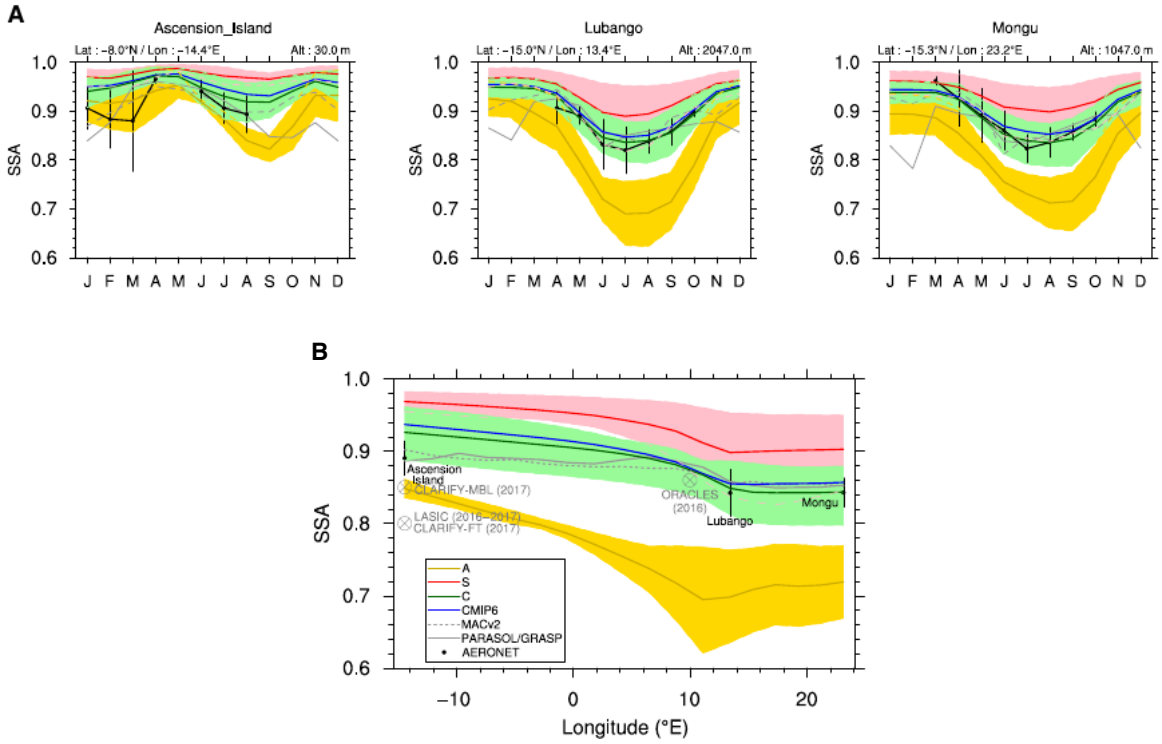

Fig. 2. Measurement compilation of aerosol SSA reveals that the CMIP6 models underestimate the smoke absorption over SEA. (**A**) SSA at 550 nm: monthly means of CMIP6 models respectively for Ascension Island, Lubango, and Mongu AERONET stations. (**B**) Averages for CMIP6 models over the transect Mongu–Lubango–Ascension Island (see Fig. 1, MACv2). For (A) and (B), the light green, red, and yellow colors represent the [10 to 90%] range for the C, S, and A CMIP6 models, respectively (see definition in Fig. 1), while the multimodel mean is in thick blue line. PARASOL/GRASP and MACv2 products have been added in gray lines for each plot. For AERONET data, the uncertainty noted with the black lines corresponds to ±1 SD. For (B), in situ SSA (550 nm) observations obtained at Ascension Island (*10*) and from the aircraft experimental campaigns [ORACLES-2016 (*27*) and CLARIFY-2017 (*6*)] have been added for comparisons. The mean SSA value for ORACLES-2016 corresponds to the "in situ" estimates (*27*).

No CMIP6 models fitted the criteria to require an A+ group (underestimated SSA and good CF).

CMIP6 models generally do not fully capture the positive direct forcing exerted by smoke over the SEA

Over the SEA, the spatial and vertical distribution of BBA must be modeled well, along with the absorption of solar radiation by BBA. Equally important in capturing the smoke direct effect is the ability to accurate representation of the underlying low-level clouds. As reported by previous studies (*7*, *8*, *10*, *39*–*42*), the direct forcing exerted by BBA over the SEA is largely positive at the top of the atmosphere during the biomass-burning season. This finding has been reinforced by remote-sensing (*9*, *43*) and regional climate model studies (*18*, *44*–*46*) associated with recent international projects, and it is clear that the SEA represents a region of the world where a persistent and intense positive solar direct aerosol effect (above clouds) diagnosed at the top of the atmosphere, which can reach ~+30 W m^{-2} (*7*, *42*, *47*).

We compared the direct radiative effect of the aerosol at top of the atmosphere (under all-sky conditions) estimated by some of the CMIP6 models (not necessarily available for all models) for the JAS season (under all-sky conditions) with MACv2 in Fig. 3A. Models classified as S− simulate a strong negative forcing of about −3 to −5 W m^{-2} over the ocean, contrary to MACv2 (−1 to +2 W m^{-2}). For these GCMs, the inconsistency with MACv2 is due to SSA overestimation (fig. S1) and a large negative bias of CF (fig. S1) that decreases the reflectance below the smoke aerosols. For models with a correct SSA but a low CF bias (C−), the forcing (~−2 W m^{-2}) is closer to that in MACv2 but still remains negative due to insufficient low-level clouds (fig. S1), which explains why they do not simulate the positive forcing over the SEA. Our results highlight that global models need to satisfactorily represent both the CF and SSA (C+) to simulate a positive forcing over the SEA that is comparable to the MACv2 data and other recent results with higher estimates (~+5/10 W m^{-2}). This conclusion agrees with former studies (*10*, *48*) that indicated the large direct forcing sensitivity to absorbing properties of smoke aerosols, clouds, and surface parameters. This leads to a dipole-like pattern in the distribution of direct forcing by MACv2, with positive forcing over the stratocumulus clouds off the coast of Southern Africa and negative forcing over the Gulf of Guinea. This pattern is only captured by the C+ models, which comprise only ~15% of the CMIP6 models. MACv2 also shows a smaller region of positive forcing over the African continent in the region of Gabon where the presence of low clouds causes the forcing to become positive (*18*)), but again, this is only reproduced by the C+ models. It should be noted that some differences in the magnitude of the modeled direct effect may also be related to the AOD (fig. S2) in addition to cloud properties and smoke SSA (*48*).

To further explore this finding, the forcing at the top of the atmosphere along the transect from Southern Africa to the tropical

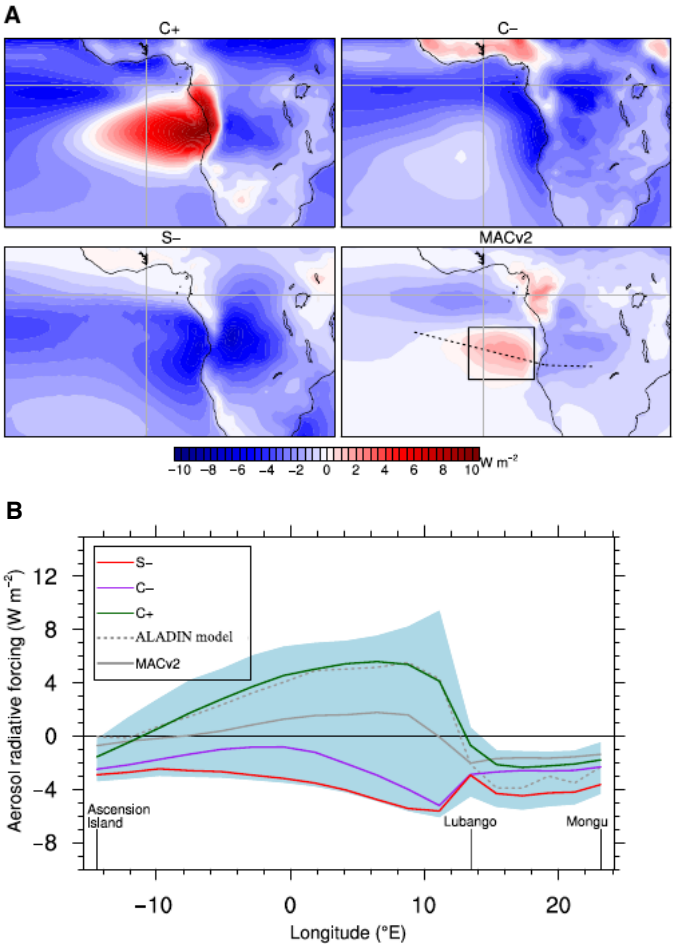

Fig. 3. Aerosol direct radiative effect at the top of the atmosphere (all-sky conditions) averaged for the JAS period. (**A**) Aerosol direct radiative effect (W m^{-2}, JAS) for C+, C–, S– CMIP6 models and from MACv2 dataset. (**B**) Direct radiative effect (W m^{-2}) for C+, C–, S– CMIP6 models, MACv2 dataset and from the recent ALADIN regional simulation [12-km horizontal resolution using smoke SSA of 0.85 at 550 nm (*18*)] averaged over the transect Mongu–Lubango–Ascension Island AERONET stations. The light blue color represents the [10 to 90%] range among CMIP6 models. ALADIN and MACv2 datasets are shown in gray.

Atlantic is shown in Fig. 3B. This indicates predominantly negative values above the continent for all the CMIP6 model groups with the largest negative values (~−4 W m^{-2}) as expected from S– models (more scattering smoke). Over the ocean (longitudes west of ~14°E), there is more variability in the sign (negative to positive) of the forcing with MACv2 and C+ models simulating a mostly positive radiative effect, while C– and S– models simulate a strong negative radiative effect. The direct effect can reach ~+4 to 8 W m^{-2} for the C+ models between 14°E and 0°, which is higher than MACv2, which reaches a maximum value of ~+2 W m^{-2}. Part of this difference is due to the higher AOD in C+ models (see fig. S2). We also note that the results from the C+ models agree with recent values obtained by a regional climate model extensively evaluated using ORACLES-2016 data (*18*, *45*). For the S– and C– model categories, the forcing is always negative, between ~−2/−6 W m^{-2} (S–) and ~−1/−4 W m^{-2} (C–), and so remains the opposite sign to the MACv2 data. Unfortunately, the direct forcing is not available for all CMIP6 models, but as most of them have showed some limitations in reproducing the low smoke SSA, particularly for the downwind regions (Figs. 1 and 2B and fig. S1), as well as low biases in CF (figs. S1 and S3), we argue here that most of those not producing forcing would likely tend toward being "too scattering" (i.e., too much cooling) over a large part of the Atlantic ocean during the biomass-burning season, with large implications for the regional climate (radiation, clouds, and precipitation).

The solar absorption and atmospheric heating induced by BBA is generally underestimated over the SEA

We evaluate the CMIP6 models further by comparing the solar absorption with Clouds and the Earth's Radiant Energy System (CERES) data (Fig. 4A) for the JAS period with the models grouped as described above (the results for all individual CMIP6 models are reported in fig. S4). We find that the error is relatively weak for C+ models but considerably higher for all other model groups. Comparisons between C+ and S+ isolate the role of BBA SSA and underline a significant low bias in absorption arises in models that do not capture low SSA (S), compared to those that represent the absorbing properties of smoke correctly (C). For the S+ models, the more scattering nature of the aerosol leads to considerable biases in solar absorption ~−30/−40 W m^{-2} over the continent and ocean and demonstrates the strong impact of underrepresenting smoke aerosol absorption in the CMIP6 GCMs. In addition to biases in the SSA, the difference between C+ and S+ models may also result from differences in AOD (fig. S2). The transect of solar absorption (Fig. 4B) shows that, over the ocean (beyond 14°E), no model is able to match the overall level of solar absorption estimated by CERES. All the CMIP6 models have less absorption except for a few C+ models and at only limited points along the transect. The bias in solar absorption is considerable over the ocean and comprised between ~−15 and −25 W m^{-2} for the CMIP6 model average. The S– models represent of about ~40% of the CMIP6 models, and for these, the bias in solar absorption reaches around ~−20 W m^{-2} over the SEA.

Directly linked to the solar absorption, the BBA-induced heating within the smoke layer, which CALIOP observations (*38*) reveal resides between 2 and 5 km, needs to be represented with fidelity in GCMs (*49*). Unlike other variables, the heating rate is not derived by MACv2, but other studies have all consistently shown pronounced radiative heating in the smoke layer with the contribution from BBA being much more important than the radiative heating associated with solar absorption by water vapor. The studies by Wilcox (*19*) or Gordon *et al.* (*44*) have indicated that the heating rate peaks can reach as high as ~2.0 to 3.5 K day^{-1} within the aerosol smoke layers for AOD near unity. A more recent study (*20*) showed absorbing aerosols leading to a significant warming of approximately 6 K day^{-1}. Solar heating rates of ~1.5 K day^{-1} (at ~650 hPa; September-October diurnal mean) have been estimated at St. Helena (*50*).

The vertical profiles of heating (Fig. 5) show that a strong heating rate perturbation is only obtained in C+ models, with the JAS mean rate rising to ~1.6 K day^{-1} between 3 and 4 km, which falls within the range of referenced estimates (*19*, *50*) (the results for all CMIP6 models are reported in fig. S5). We also find that for C– models, which reasonably represent SSA, heating is still too low due to the poor representation of stratocumulus clouds, which limits the interaction between solar fluxes reflected by clouds and absorbing smoke. As expected, the lowest heating rate for the region

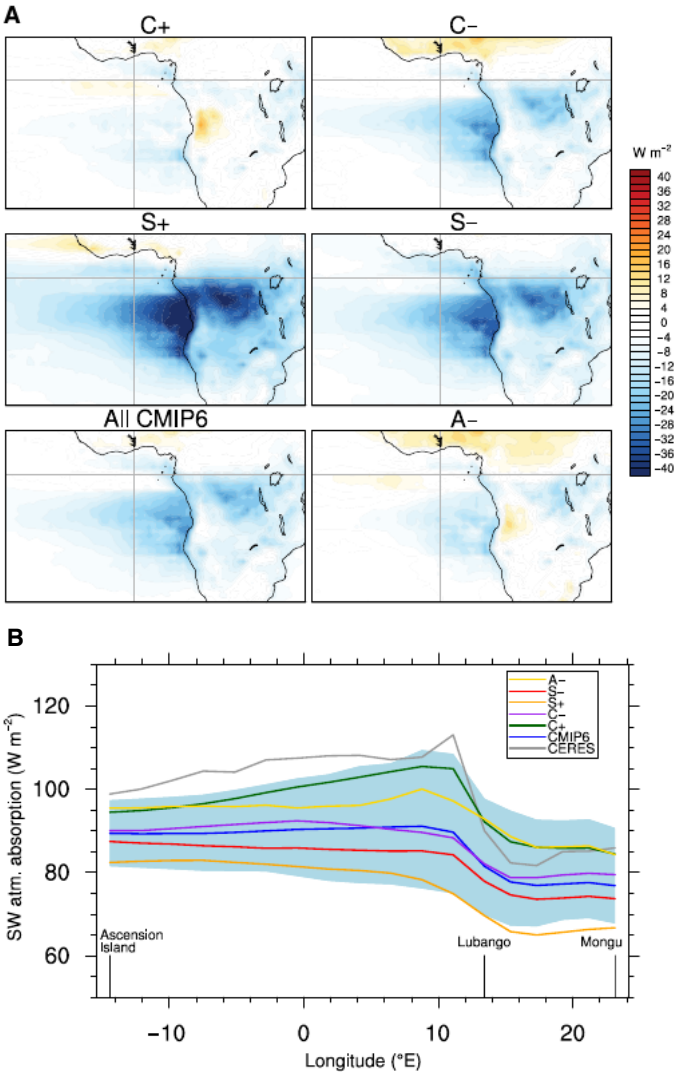

Fig. 4. Averaged shortwave atmospheric absorption (W m^{-2}) for the JAS period. (**A**) Bias in shortwave atmospheric absorption for C+, C−, S−, S+, A−, and all CMIP6 models against the CERES dataset. (**B**) Shortwave atmospheric absorption (W m^{-2}, JAS average) for C+, C−, S−, S+, A−, and all CMIP6 models averaged over the transect Mongu–Lubango–Ascension Island. For (B), the light blue color represents the [10 to 90%] range for CMIP6 models. CERES data are shown in gray in (B).

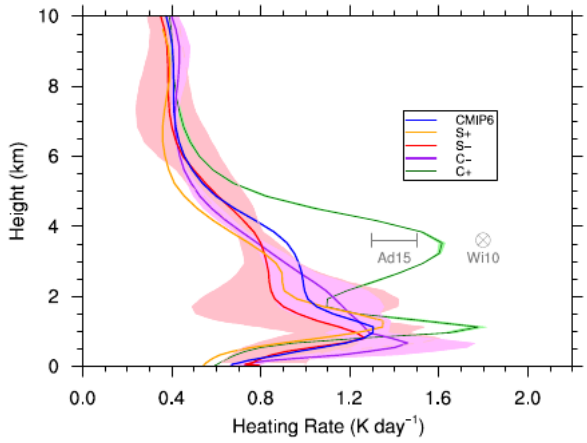

Fig. 5. Averaged shortwave heating rate (K day^{-1}) over the SEA for the JAS period. SW heating rate in S+, S−, C+, C−, and all CMIP6 models (averaged over the box 3°W/11°E-7°S/18°S). The light green, red, and purple colors represent the [10 to 90%] range for C+, S−, and C− CMIP6 models. SW heating rates (under all-sky conditions) obtained in (*19*) (Wi10)] and (*50*) (Ad15) have been added for comparison. For Wi10, the estimate is based on radiative transfer simulations using satellite (CALIOP, OMI, and MODIS) data]. Aerosols are distributed from 1.5 to 4.0 km over the SEA with peak concentration at ~3-km altitude. Absorbing properties (SSA of 0.89 at 550 nm) are derived from SAFARI 2000. The reported solar heating corresponds to AOD of 0.4 (550 nm), CF of 1, and cloud optical depth of 12. For Ad15, estimates are based on radiative transfer simulations. The value reported corresponds to September-October (diurnal mean) heating rate at St. Helena for cloudy cases (interval values are reported for two different cloud optical depth; 5 and 15) averaged over all available AOD (fine), assuming an SSA of 0.86 and for moist background thermodynamic profiles.

at around 3 km (~0.8 K day^{-1}) is obtained for the S− models due to the low surface albedo and overly scattering smoke. This appears too low compared to the evidence from previous studies (Fig. 5), and we hypothesize that the solar heating from the smoke is underestimated over the SEA because most (~75%) of the CMIP6 models have significant bias in SSA and CF over the ocean.

DISCUSSION

Implications for the SEA regional climate

Although important uncertainties remain in quantifying the semidirect effect by absorbing aerosols (*14*), there seems to be a consensus on how this process acts over the SEA. Several studies, based on large eddy simulations (*15*, *16*), global/regional climate models (*10*, *17*, *18*, *51*), and observations (*19*, *20*), all indicate that BBA generally reinforces the low-level cloud cover in this region. The main driving process is identified as the additional radiative heating generated by smoke above the low-level clouds, which increases the stability of the low-level inversion limiting the entrainment of dry air from the free troposphere to the marine boundary layer. As shown previously, this key radiative feedback is not properly represented in many CMIP6 models, and the heating rates induced by smoke are likely to be generally too weak. In their current configurations, we hypothesis that the cloud adjustments are probably too weak in most of the models due to underrepresenting the absorption by smoke over the SEA, and this could lead to an underestimate of the semidirect forcing by BBA. The sensitivity study of Johnson *et al.* (*15*) highlights this relationship, showing that the absorbing smoke properties can have a significant impact on semidirect forcing, with the radiative adjustment ranging from −9.5 to +0.1 W m^{-2} (at the top of the atmosphere) for absorbing to scattering smoke. This shows that a misrepresentation of these feedbacks on stratocumulus clouds could potentially have important climatic impacts as modest increases in the cloud coverage, liquid water content, and decreases of the size droplet are able to produce a radiative effect that could balance the forcing due to doubled carbon dioxide concentrations (*22*). Not taking into account the semidirect forcing may also have large implications on the surface energy budget. As shown in (*10*) or more recently in (*18*), both the cloud adjustment (increase in low cloudiness) due to the semidirect forcing of smoke aerosols, together with their own dimming effect,

significantly decrease downwelling solar radiation at the surface and hence the sea surface temperature (SST) (by ~1 to 1.5 K) over a large part of the tropical Atlantic ocean. This BBA/low-clouds/SST feedback loop could also possibly contribute to the persistent warm SST bias detected in CMIP6 models over the tropical Atlantic (*33*).

The hydrological cycle is another important consideration as recent studies (*25*, *26*) have underlined possible links between BBA radiative effects and precipitation over the Western African monsoon region. All three studies report a precipitation decrease over the Northern Gulf of Guinea (by ~2 mm per day during JAS period) due to fast adjustments associated with surface cooling and atmospheric heating by transported BBA that increase the lower tropospheric stability. In both studies, atmospheric heating (BBA solar absorption) and SST anomalies (BBA surface dimming and cloud adjustments) are identified as key processes intrinsically linked to absorbing properties of smoke. These recent (*25*, *26*) results underline that insufficient absorption by smoke over the tropical ocean in global models would limit these interactions between BBA and the fast responses of precipitation (drying) over the southern West Africa. In addition, even if the SSA bias appears to be less pronounced over the African continent, the drying effect of absorbing smoke over central Africa (*24*) would not be fully represented for CMIP6 models with too scattering BBA over the continent (Fig. 1). It is important to note that even CMIP6 C+ models, which simulate both the cloud cover and BBA absorption properties reasonably well, still retain important biases in solar radiation absorption both over the SEA (±5 W m^{-2}) and the continent (~10 to 20 W m^{-2}) (Fig. 4, A and B). Even for this group (C+) of the models, the low cloud feedbacks and responses of precipitation due to BBA radiative forcing could still be underestimated.

Another concern is that the possible "self-lofting" mechanism (*52*) would not be fully captured in GCMs if absorption is too weak. This potentially has large implications for the vertical profiles, long-range transport, and radiative effects of smoke. If atmospheric conditions are favorable, strongly absorbing BBA are known to heat the atmospheric layer where they are located and this could gently lift smoke aerosols to higher altitudes by increasing the upward vertical velocity or decreasing the subsidence within the plume. A recent study (*53*) indicated that smoke-induced heating could elevate the BBA plume by about 1 km over the SEA. Because of the large underestimate of SSA by most CMIP6 models during the transport, we argue that the self-lofting process is probably too weak in models and may explain part of the bias in the BBA extinction vertical profiles (*38*). Advecting smoke to higher altitudes could potentially increase the above-cloud AOD and the related direct forcing of the smoke, modulate the semidirect effect, and reduce or prevent the mixing of BBA into the marine boundary layer, thus also modulating the indirect effect of smoke plumes over the SEA.

Possibilities for improving the solar absorption by BBA in global climate models

There may be several reasons why the CMIP6 models underestimate the aerosol solar absorption over the SEA. First, this may be due to an underestimation of the concentration of the smoke itself. It is now recognized that emission inventories do not enable models to adequately represent the concentration and AOD of smoke aerosols; very often, modelers have to scale BBA emissions for black carbon (BC) and organic carbon (OC) by a factor between 1.5 and 6 to simulate realistic satellite AOD over biomass burning regions (*54*). This problem could be due to difficulties in satellite retrievals in detecting subpixel fires (*55*). In CMIP6 models, this could explain part of the identified negative bias in AOD (fig. S2), which could also contribute to the underestimate of the solar absorption. Another reason could be that the height of smoke layers decreases too quickly in climate models, explaining the insufficient long-range transport of the BBA plume over the Atlantic (*38*). This underestimate in the altitude of transport could favor stronger uptake of water or sulfate from dimethyl sulfide as the aerosol ages and entrains into the boundary layer (BL), leading to faster removal by wet deposition and an aerosol mixture with higher SSA.

A second possibility is that the aerosol chemical composition and refractive index could be inadequately represented in some of the models, as these factors are fundamental in calculating the optical properties. For instance, studies have shown that the aerosol SSA over the SEA is better reproduced by models that use a high imaginary part of the refractive index [0.71 at 550 nm (*56*)] for black carbon (*57*). The way in which the mixing state of aerosols (internal/external) that takes place during aging is taken into account in CMIP6 models has to also be considered as it significantly modulates the absorption efficiency of BBA (*58*). A recent study has indicated more complex mixing states than those used in global modeling (many still assume external mixing or volume weighting of the refractive index in internal mixtures), which may explain the strong solar absorption by smoke over the SEA (*59*). Another explanation is the neglect or underestimation of absorption by the organic matter, which makes up most of the aerosol mass in BBA plumes and may itself change with aging (*6*, *59*, *60*). This absorbing organic component or so-called brown carbon is not included in all models (*60*) and failing to do so could contribute to the low bias of solar absorption in this region. Last, the evaporation of organics or the condensation of nitrates at higher altitudes as BBA plume age (about 1 or 2 days after emissions) could modulate the SSA (*6*), but these processes of aging are not represented in the CMIP6 models.

Global climate models must account for the large absorption of smoke aerosols over the SEA to accurately simulate their direct radiative effect at top of atmosphere (TOA), the changes of low clouds, the altitude of transport, and the fast precipitation responses. We demonstrate that most of the latest versions of CMIP6 climate models underestimate the strong solar absorption by BBA over the SEA that has been consistently highlighted by recent experimental campaigns, new satellite observations, and a recent climatological aerosol dataset. We find that many CMIP6 models do not adequately represent the intense positive (warming) radiative effect exerted at the top of the atmosphere by smoke, and we highlight the crucial role played by both the representation of low clouds and the absorption properties of BBA in such a bias. The implication is that the BBA-induced radiative heating will also be underestimated, suggesting that the increase of the low-level clouds due to the semidirect effect of smoke is probably too weak. Another possible consequence is that the drying effect by BBA recently highlighted over the densely populated southern West African region may not be well captured, as this aerosol-climate feedback appears to be linked to lower troposphere heating due to smoke. Considering all of the possible implications on the SEA regional climate (radiative budget, cloudiness, and precipitation), further development of parametrizations in climate models is needed to improve the representation of this key radiative property in the next generation of GCMs. This is needed to correctly simulate the present and future

climate of this region, which has been subject to strong variability in smoke aerosol emissions over the last 50 years (*24*). These developments will benefit from the unique in situ and remote-sensing observations acquired recently over the SEA (CLARIFY-2017, ORACLES, LASIC, DACCIWA, and AEROCLO-sA).

MATERIALS AND METHODS

CMIP6 SW absorption and SSA calculations

An ensemble of 62 CMIP6 models [e.g., organized by the World Climate Research Programme (WCRP), participating models will contribute to the assessment of 2024 Intergovernmental Panel on Climate Change (IPCC)] has been used in the present study, the selection relying on the availability of the required variables. Among them, 38 models are used in the analysis of the effect of aerosol absorption thanks to the availability of the abs550aer variable. Monthly means of AOD (od550aer), absorption AOD (abs550aer), CF (clt), surface (rsds) and top of the atmosphere (rsut) shortwave radiation, and tendency of air temperature due to shortwave radiative heating (tntrs) coming from the CMIP6 historical simulation have been downloaded from the ESGF (Earth System Grid Federation) nodes from which the JAS average has been calculated over the 1995–2014 period. Shortwave (SW) atmospheric absorption has been calculated as the difference between TOA and surface radiation, while aerosol SSA is inferred from AOD and absorption AOD (where AAOD = AOD − (1 − SSA).

For the analysis, models have been classified in different categories according to their biases in SSA and CF over the SEA region. These biases are calculated over the box 3°W to 11°E and 7°S to 18°S. For SSA, the bias is calculated with regards to the MACv2 dataset, and three categories are defined: "correct (C)" for models with bias lesser than 0.04, "scattering (S)" for positive bias higher than 0.04, and "absorbing (A)" for negative bias lower than −0.04. For CF, the bias is computed against the CALIOP dataset and two categories are defined: correct (noted +) for bias in CF ≤ 25% (over the box 3°W to 11°E 7° to 18°S) or poor (noted −) for CF bias > 25%. By merging the two variables, five groups (table S1) of models are analyzed: C+ (for correct SSA and good CF), C− (correct SSA/poor CF), S+ (overestimated SSA/good CF), S− (overestimated SSA/poor CF), and A− (underestimated SSA/poor CF).

Evaluation

Observation data

The second aerosol dataset used in this paper is the 2017 version of the Max Planck Institute Aerosol Climatology [MACv2 (*31*)], which is an update of the MAC-v1 climatology. This dataset provides monthly aerosol optical properties on a 1° grid, derived from a combination of observations and model outputs. MACv2 covers the 1850–2100 period and includes interannual variability for the anthropogenic aerosols, while natural aerosols consider only monthly variations. Optical properties for the main aerosol types (i.e., dust, sea salt, black carbon, organic matter, and sulfate) are provided. AERONET stations have been used to evaluate the SSA at 550 nm. Observations include the AERONET ground-based sun photometers network (http://aeronet.gsfc.nasa.gov), as well as measurements over ocean provided by the Maritime Aerosol Network (*61*). The SSA has been calculated from AOD and absorption AOD available at 440 or 500 nm and then converted to 550 nm using the angström exponent (i.e., spectral dependence of AOD). For each station, only months where 8 days of measurements were available from at least 3 years have been kept. The resulting dataset has then been compared to each model output of SSA, interpolated to the location of the station.

Satellite data

We used aerosol products obtained by the GRASP algorithm from POLDER/PARASOL observations. GRASP is a new algorithm that allows retrieval of aerosol and surface properties from diverse remote-sensing observations [see detailed description in (*62*, *63*)]. GRASP has been used for processing the full archive (2005–2013) of POLDER-3/PARASOL observations to produce PARASOL/GRASP aerosol data products. These level 3 0.1° products were validated using AERONET data and comparisons with moderate resolution imaging spectroradiometer (MODIS) products (*30*). The results showed that the PARASOL/GRASP retrieval provided reliable aerosol products and important advances over the reference MODIS aerosol products. Specifically, GRASP/Models products (that is overall the best among other POLDER products such as POLDER/Operational, GRASP/high precision (HP), and GRASP/Optimized) provided spectral AOD with the highest correlations globally and smallest biases compared to all PARASOL and MODIS datasets. In this study, we use GRASP/Model PARASOL products, named as PARASOL/GRASP. These satellite products provided detailed aerosol properties including AOD of fine and coarse mode, angström exponent, AOD of absorption, and SSA both over land and ocean. Many of these retrieval products are not available from other instruments. Figure S6 illustrates GRASP/Models validation of SSA over several AERONET sites in central Africa, including Djougou, Mongu, Mongu Inn, and Ascension Island. In addition, Schutgens *et al.* (*64*) have evaluated GRASP/Models SSA against AERONET and compared with other satellite SSA products. The study recognized GRASP/Models as one of the most reliable and extensive available datasets of aerosol SSA. It has many more retrieved values globally compared to other products and showed the best correlation with AERONET data. We have followed the same strategy as presented in (*30*) for GRASP/Models data quality assurance and AERONET matchup methodology. Briefly, we averaged satellite retrievals in a 3 km × 3 km window over land and a 9 km × 9 km window over ocean for the gridded satellite data centered over the AERONET sites; meanwhile, the available AERONET inversion products are averaged within ±180 min of the PARASOL overpass.

Observed CF is obtained from the CALIOP (*65*) lidar aboard CALIPSO flying in the A-Train constellation. At the top of the atmosphere, shortwave radiation is evaluated against the CERES–Energy Balanced and Filled data (*66*) in version 2.8 at 1° resolution over the 2000–2016 period.

SUPPLEMENTARY MATERIALS

Supplementary material for this article is available at https://science.org/doi/10.1126/sciadv.abg9998

REFERENCES AND NOTES

1. P. Zuidema, A. J. Sedlacek III, C. Flynn, S. Springston, R. Delgadillo, J. Zhang, A. Aiken, A. Koontz, P. Muradyan, The Ascension Island boundary layer in the remote southeast Atlantic is often smoky. *Geophys. Res. Lett.* **45**, 4456–4465 (2018).
2. C. Flamant, P. Knippertz, A. Fink, A. Akpo, B. J. Brooks, C. J. Chiu, H. Coe, S. Danuor, M. J. Evans, O. Jegede, N. Kalthoff, A. Konaré, C. Liousse, F. Lohou, C. Mari, H. Schlager, A. Schwarzenboeck, B. Adler, L. Amekudzi, J. Aryee, M. Ayoola, A. M. Batenburg, G. Bessardon, S. Borrmann, J. Brito, K. Bower, F. Burnet, V. Catoire, A. Colomb, C. Denjean, K. Fosu-Amankwah, P. G. Hill, J. Lee, M. Lothon, M. Maranan, J. Marsham, R. Meynadier,

J.-B. Ngamini, P. Rosenberg, D. Sauer, V. Smith, G. Stratmann, J. W. Taylor, C. Voigt, V. Yoboué, The Dynamics–Aerosol–Chemistry–Cloud Interactions in West Africa field campaign: Overview and research highlights. *Bull. Am. Meteorol. Soc.* **99**, 83–104 (2018).
3. J. Redemann, R. Wood, P. Zuidema, S. J. Doherty, B. Luna, S. E. LeBlanc, M. S. Diamond, Y. Shinozuka, I. Y. Chang, R. Ueyama, L. Pfister, J. Ryoo, A. N. Dobracki, A. M. da Silva, K. M. Longo, M. S. Kacenelenbogen, C. J. Flynn, K. Pistone, N. M. Knox, S. J. Piketh, J. M. Haywood, P. Formenti, M. Mallet, P. Stier, A. S. Ackerman, S. E. Bauer, A. M. Fridlind, G. R. Carmichael, P. E. Saide, G. A. Ferrada, S. G. Howell, S. Freitag, B. Cairns, B. N. Holben, K. D. Knobelspiesse, S. Tanelli, T. S. L'Ecuyer, A. M. Dzambo, O. O. Sy, G. M. McFarquhar, M. R. Poellot, S. Gupta, J. R. O'Brien, A. Nenes, M. E. Kacarab, J. P. S. Wong, J. D. Small-Griswold, K. L. Thornhill, D. Noone, J. R. Podolske, K. S. Schmidt, P. Pilewskie, H. Chen, S. P. Cochrane, A. J. Sedlacek, T. J. Lang, E. Stith, M. Segal-Rozenhaimer, R. A. Ferrare, S. P. Burton, C. A. Hostetler, D. J. Diner, S. E. Platnick, J. S. Myers, K. G. Meyer, D. A. Spangenberg, H. Maring, L. Gao, An overview of the ORACLES (ObseRvations of Aerosols above CLouds and their intEractionS) project: Aerosol–cloud–radiation interactions in the Southeast Atlantic basin. *Atmos. Chem. Phys.* **21**, 1507–1563 (2021).
4. J. M. Haywood, S. J. Abel, P. A. Barrett, N. Bellouin, A. Blyth, K. N. Bower, M. Brooks, K. Carslaw, H. Che, H. Coe, M. I. Cotterell, I. Crawford, Z. Cui, N. Davies, B. Dingley, P. Field, P. Formenti, H. Gordon, M. de Graaf, R. Herbert, B. Johnson, A. C. Jones, J. M. Langridge, F. Malavelle, D. G. Partridge, F. Peers, J. Redemann, P. Stier, K. Szpek, J. W. Taylor, D. Watson-Parris, R. Wood, H. Wu, P. Zuidema, Overview: The CLoud–Aerosol–Radiation interaction and forcing: Year-2017 (CLARIFY-2017) measurement campaign. *Atmos. Chem. Phys.* **21**, 1049–1084 (2021).
5. P. Formenti, B. D'Anna, C. Flamant, M. Mallet, S. Piketh, K. Schepanski, F. Waquet, F. Auriol, G. Brogniez, F. Burnet, J. P. Chaboureau, A. Chauvigné, P. Chazette, C. Denjean, K. Desboeufs, J. Doussin, N. Elguindi, S. Feuerstein, M. Gaetani, C. Giorio, D. Klopper, M. Mallet, P. Nabat, A. Monod, F. Solmon, A. Namwoonde, C. Chikwililwa, R. Mushi, E. Welton, B. Holben, The Aerosols, Radiation and Clouds in Southern Africa field campaign in Namibia: Overview, illustrative observations, and way forward. *Bull. Am. Meteorol. Soc.* **100**, 1277–1298 (2019).
6. H. Wu, J. W. Taylor, K. Szpek, J. M. Langridge, P. I. Williams, M. Flynn, J. D. Allan, S. J. Abel, J. Pitt, M. I. Cotterell, C. Fox, N. W. Davies, J. Haywood, H. Coe, Vertical variability of the properties of highly aged biomass burning aerosol transported over the southeast Atlantic during CLARIFY-2017. *Atmos. Chem. Phys.* **20**, 12697–12719 (2020).
7. M. de Graaf, N. Bellouin, L. G. Tilstra, J. Haywood, P. Stammes, Aerosol direct radiative effect of smoke over clouds over the southeast Atlantic Ocean from 2006 to 2009. *Geophys. Res. Lett.* **41**, 7723–7730 (2014).
8. N. Feng, S. A. Christopher, Measurement-based estimates of direct radiative effects of absorbing aerosols above clouds. *J. Geophys. Res.-Atmos.* **120**, 6908–6921 (2015).
9. M. S. Kacenelenbogen, M. A. Vaughan, J. Redemann, S. A. Young, Z. Liu, Y. Hu, A. H. Omar, S. LeBlanc, Y. Shinozuka, J. Livingston, Q. Zhang, K. A. Powell, Estimations of global shortwave direct aerosol radiative effects above opaque water clouds using a combination of A-Train satellite sensors. *Atmos. Chem. Phys.* **19**, 4933–4962 (2019).
10. N. Sakaeda, R. Wood, P. J. Rasch, Direct and semi-direct aerosol effects of southern African biomass burning aerosol. *J. Geophys. Res.* **116**, D12205 (2011).
11. P. Zuidema, J. Redemann, J. Haywood, R. Wood, S. Piketh, M. Hipondoka, P. Formenti, Smoke and clouds above the southeast Atlantic: Upcoming field campaigns probe absorbing aerosol's impact on climate. *B. Am. Meteorol. Soc.* **97**, 1131–1135 (2016).
12. P. Stier, N. A. J. Schutgens, N. Bellouin, H. Bian, O. Boucher, M. Chin, S. Ghan, N. Huneeus, S. Kinne, G. Lin, X. Ma, G. Myhre, J. E. Penner, C. A. Randles, B. Samset, M. Schulz, T. Takemura, F. Yu, H. Yu, C. Zhou, Host model uncertainties in aerosol radiative forcing estimates: Results from the AeroCom Prescribed intercomparison study. *Atmos. Chem. Phys.* **13**, 3245–3270 (2013).
13. A. S. Ackerman, O. B. Toon, D. E. Stevens, A. J. Heymsfield, V. Ramanathan, E. J. Welton, Reduction of tropical cloudiness by Soot. *Science* **288**, 1042–1047 (2000).
14. D. Koch, A. D. Del Genio, Black carbon semi-direct effects on cloud cover: Review and synthesis. *Atmos. Chem. Phys.* **10**, 7685–7696 (2010).
15. B. T. Johnson, K. P. Shine, P. M. Forster, The semi-direct aerosol effect: Impact of absorbing aerosols on marine stratocumulus. *Q. J. Roy. Meteorol. Soc.* **130**, 1407–1422 (2004).
16. R. J. Herbert, N. Bellouin, E. J. Highwood, A. A. Hill, Diurnal cycle of the semi-direct effect from a persistent absorbing aerosol layer over marine stratocumulus in large-eddy simulations. *Atmos. Chem. Phys.* **20**, 1317–1340 (2020).
17. C. Randles, V. Ramaswamy, Direct and semi-direct impacts of absorbing biomass burning aerosol on the climate of southern Africa: A Geophysical Fluid Dynamics Laboratory GCM sensitivity study. *Atmos. Chem. Phys.* **10**, 9819–9831 (2010).
18. M. Mallet, F. Solmon, P. Nabat, N. Elguindi, F. Waquet, D. Bouniol, A. M. Sayer, K. Meyer, R. Roehrig, M. Michou, P. Zuidema, C. Flamant, J. Redemann, P. Formenti, Direct and semi-direct radiative forcing of biomass-burning aerosols over the Southeast Atlantic (SEA) and its sensitivity to absorbing properties: A regional climate modeling study. *Atmos. Chem. Phys.* **20**, 13191–13216 (2020).
19. E. Wilcox, Direct and semi-direct radiative forcing of smoke aerosols over clouds. *Atmos. Chem. Phys.* **12**, 139–149 (2012).
20. L. T. Deaconu, N. Ferlay, F. Waquet, F. Peers, F. Thieuleux, P. Goloub, Satellite inference of water vapour and above-cloud aerosol combined effect on radiative budget and cloud-top processes in the southeastern Atlantic Ocean. *Atmos. Chem. Phys.* **19**, 11613–11634 (2019).
21. Z. Lu, X. Liua, Z. Zhang, C. Zhao, K. Meyer, C. Rajapakshe, C. Wu, Z. Yang, J. E. Penner, Biomass smoke from southern Africa can significantly enhance the brightness of stratocumulus over the southeastern Atlantic Ocean. *Proc. Natl. Acad. Sci. U.S.A.* **115**, 2924–2929 (2018).
22. A. Slingo, Sensitivity of the Earth's radiation budget to changes in low clouds. *Nature* **343**, 49–51 (1990).
23. M. G. Tosca, D. J. Diner, M. J. Garay, O. V. Kalashnikova, Human-caused fires limit convection in tropical Africa: First temporal observations and attribution. *Geophys. Res. Lett.* **42**, 6492–6501 (2015).
24. Ø. Hodnebrog, G. Myhre, P. M. Forster, J. Sillmann, B. H. Samset, Local biomass burning is a dominant cause of the observed precipitation reduction in southern Africa. *Nat. Commun.* **7**, 11236 (2016).
25. O. Ajoku, J. R. Norris, A. J. Miller, Observed monsoon precipitation suppression caused by anomalous interhemispheric aerosol transport. *Clim. Dynam.* **54**, 1077–1091 (2019).
26. G. Pante, P. Knippertz, A. H. Fink, A. Kniffka, The potential of increasing man-made air pollution to reduce rainfall over southern West Africa. *Atmos. Chem. Phys.* **21**, 35–55 (2021).
27. K. Pistone, J. Redemann, S. Doherty, P. Zuidema, S. Burton, B. Cairns, S. Cochrane, R. Ferrare, C. Flynn, S. Freitag, S. G. Howell, M. Kacenelenbogen, S. LeBlanc, X. Liu, S. Schmidt, A. J. Sedlacek, M. Segal-Rozenhaimer, Y. Shinozuka, S. Stamnes, B. van Diedenhoven, G. Van Harten, G. F. Xu, Intercomparison of biomass burning aerosol optical properties from in situ and remote-sensing instruments in ORACLES-2016. *Atmos. Chem. Phys.* **19**, 9181–9208 (2019).
28. C. Denjean, T. Bourrianne, F. Burnet, M. Mallet, N. Maury, A. Colomb, P. Dominutti, J. Brito, R. Dupuy, K. Sellegri, A. Schwarzenboeck, C. Flamant, P. Knippertz, Overview of aerosol optical properties over Southern West Africa from DACCIWA aircraft measurements. *Atmos. Chem. Phys.* **20**, 4735–4756 (2020a).
29. N. W. Davies, C. Fox, K. Szpek, M. I. Cotterell, J. W. Taylor, J. D. Allan, P. I. Williams, J. Trembath, J. M. Haywood, J. M. Langridge, Evaluating biases in filter-based aerosol absorption measurements using photoacoustic spectroscopy. *Atmos. Meas. Tech.* **12**, 3417–3434 (2019).
30. C. Chen, O. Dubovik, D. Fuertes, P. Litvinov, T. Lapyonok, A. Lopatin, F. Ducos, Y. Derimian, M. Herman, D. Tanré, L. A. Remer, A. Lyapustin, A. M. Sayer, R. C. Levy, N. C. Hsu, J. Descloitres, L. Li, B. Torres, Y. Karol, M. Herrera, M. Herreras, M. Aspetsberger, M. Wanzenboeck, L. Bindreiter, D. Marth, A. Hangler, C. Federspiel, Validation of GRASP algorithm product from POLDER/PARASOL data and assessment of multi-angular polarimetry potential for aerosol monitoring. *Earth Syst. Sci. Data* **12**, 3573–3620 (2020).
31. S. Kinne, Aerosol radiative effects with MACv2. *Atmos. Chem. Phys.* **19**, 10919–10959 (2019).
32. H. Brown, X. Liu, R. Pokhrel, S. Murphy, Z. Lu, R. Saleh, T. Mielonen, H. Kokkola, T. Bergman, G. Myhre, R. B. Skeie, D. Watson-Paris, P. Stier, B. Johnson, N. Bellouin, M. Schulz, V. Vakkari, J. P. Beukes, P. G. van Zyl, S. Liu, D. Chand, Biomass burning aerosols in most climate models are too absorbing. *Nat. Commun.* **12**, 277 (2021).
33. F. Hourdin, A. Găinuşă-Bogdan, P. Braconnot, J.-L. Dufresne, A.-K. Traore, A.-K. Traore, C. Rio, Air moisture control on ocean surface temperature, hidden key to the warm bias enigma. *Geophys. Res. Lett.* **42**, 10,885–10,893 (2015).
34. B. H. Samset, G. Myhre, P. M. Forster, Ø. Hodnebrog, T. Andrews, G. Faluvegi, D. Fläschner, M. Kasoar, V. Kharin, A. Kirkevåg, J. F. Lamarque, D. Olivié, T. Richardson, D. Shindell, K. P. Shine, T. Takemura, A. Voulgarakis, Fast and slow precipitation responses to individual climate forcers: A PDRMIP multimodel study. *Geophys. Res. Lett.* **43**, 2782–2791 (2016).
35. B. N. Holben, T. F. Eck, I. Slutsker, D. Tanré, J. P. Buis, A. Setzer, E. Vermote, J. A. Reagan, Y. Kaufman, T. Nakajima, F. Lavenu, I. Jankowiak, A. Smirnov, AERONET—A federated instrument network and data archive for aerosol characterization. *Remote Sens. Environ.* **66**, 1–16 (1998).
36. O. Dubovik, B. Holben, T. F. Eck, A. Smirnov, Y. J. Kaufman, M. D. King, D. Tanre, I. Slutsker, Variability of absorption and optical properties of key aerosol types observed in worldwide locations. *J. Atmos. Sci.* **59**, 590–608 (2002).
37. T. F. Eck, B. N. Holben, J. S. Reid, M. M. Mukelabai, S. J. Piketh, O. Torres, H. T. Jethva, E. J. Hyer, D. E. Ward, O. Dubovik, A. Sinyuk, J. S. Schafer, D. M. Giles, M. Sorokin, A. Smirnov, I. Slutsker, A seasonal trend of single scattering albedo in southern African biomass-burning particles: Implications for satellite products and estimates of emissions for the world's largest biomass-burning source. *J. Geophys. Res. Atmos.* **118**, 6414–6432 (2013).
38. S. Das, H. Harshvardhan, M. Bian, G. Chin, A. P. Curci, T. Protonotariou, K. Mielonen, H. Zhang, H. Wang, X. Liu, Biomass burning aerosol transport and vertical distribution over the South African-Atlantic region. *J. Geophys. Res. Atmos.* **122**, 6391–6415 (2017).
39. G. Myhre, T. K. Berntsen, J. M. Haywood, J. K. Sundet, B. N. Holben, M. Johnsrud, F. Stordal, Modeling the solar radiative impact of aerosols from biomass burning during

the Southern African Regional Science Initiative (SAFARI-2000) experiment. *J. Geophys. Res.* **108**, 8501 (2003).
40. K. Meyer, S. Platnick, L. Oreopoulos, D. Lee, Estimating the direct radiative effect of absorbing aerosols overlying marine boundary layer clouds in the southeast Atlantic using MODIS and CALIOP. *J. Geophys. Res. Atmos.* **118**, 4801–4815 (2013).
41. M. Min, Z. Zhang, On the influence of cloud fraction diurnal cycle and sub-grid cloud optical thickness variability on all-sky direct aerosol radiative forcing. *J. Quant. Spectrosc. Radiat. Transf.* **142**, 25–36 (2014).
42. F. Peers, F. Waquet, C. Cornet, P. Dubuisson, F. Ducos, P. Goloub, F. Szczap, D. Tanré, F. Thieuleux, Absorption of aerosols above clouds from POLDER/PARASOL measurements and estimation of their direct radiative effect. *Atmos. Chem. Phys.* **15**, 4179–4196 (2015).
43. M. de Graaf, R. Schulte, F. Peers, F. Waquet, L. G. Tilstra, P. Stammes, Comparison of south-east Atlantic aerosol direct radiative effect over clouds from SCIAMACHY, POLDER and OMI–MODIS. *Atmos. Chem. Phys.* **20**, 6707–6723 (2020).
44. H. Gordon, P. R. Field, S. J. Abel, M. Dalvi, D. P. Grosvenor, A. A. Hill, B. T. Johnson, A. K. Miltenberger, M. Yoshioka, K. S. Carslaw, Large simulated radiative effects of smoke in the south-east Atlantic. *Atmos. Chem. Phys.* **18**, 15261–15289 (2018).
45. M. Mallet, P. Nabat, P. Zuidema, J. Redemann, A. M. Sayer, M. Stengel, S. Schmidt, S. Cochrane, S. Burton, R. Ferrare, K. Meyer, P. Saide, H. Jethva, O. Torres, R. Wood, D. Saint Martin, R. Roehrig, C. Hsu, P. Formenti, Simulation of the transport, vertical distribution, optical properties and radiative impact of smoke aerosols with the ALADIN regional climate model during the ORACLES-2016 and LASIC experiments. *Atmos. Chem. Phys.* **19**, 4963–4990 (2019).
46. H. Che, P. Stier, H. Gordon, D. Watson-Parris, L. Deaconu, Cloud adjustments dominate the overall negative aerosol radiative effects of biomass burning aerosols in UKESM1 climate model simulations over the south-eastern Atlantic. *Atmos. Chem. Phys.* **21**, 17–33 (2021).
47. S. P. Cochrane, K. S. Schmidt, H. Chen, P. Pilewskie, S. Kittelman, J. Redemann, S. LeBlanc, K. Pistone, M. Kacenelenbogen, M. Segal Rozenhaimer, Y. Shinozuka, C. Flynn, S. Platnick, K. Meyer, R. Ferrare, S. Burton, C. Hostetler, S. Howell, S. Freitag, A. Dobracki, S. Doherty, Above-cloud aerosol radiative effects based on ORACLES 2016 and ORACLES 2017 aircraft experiments. *Atmos. Meas. Tech.* **12**, 6505–6528 (2019).
48. T. J. Thorsen, R. A. Ferrare, S. Kato, D. M. Winker, Aerosol direct radiative effect sensitivity analysis. *J. Climate* **33.14**, 6119–6139 (2020).
49. J. E. Hansen, M. Sato, R. Ruedy, Radiative forcing and climate response. *J. Geophys. Res.* **102**, 6831–6864 (1997).
50. A. A. Adebiyi, P. Zuidema, S. J. Abel, The convolution of dynamics and moisture with the presence of shortwave absorbing aerosols over the southeast atlantic. *J. Climate* **28**, 1997–2024 (2015).
51. R. J. Allen, A. Amiri-Farahani, J.-F. Lamarque, C. Smith, D. Shindell, T. Hassan, C. E. Chung, Observationally-constrained aerosol–cloud semi-direct effects. *npj Clim. Atmos. Sci.* **2**, 16 (2019).
52. L. F. Radke, J. H. Lyons, P. V. Hobbs, R. E. Weiss, Smokes from the burning of aviation fuel and their self-lofting by solar heating. *J. Geophys. Res.* **95**, 14071–14076 (1990).
53. B. Johnson, J. Haywood, Self-rising aerosols, AEROCOM meeting, 2020.
54. C. L. Reddington, D. V. Spracklen, P. Artaxo, D. Ridley, L. V. Rizzo, A. Arana, Analysis of particulate emissions from tropical biomass burning using a global aerosol model and long-term surface observations. *Atmos. Chem. Phys.* **16**, 11083–11106 (2016).
55. R. Ramo, E. Roteta, I. Bistinas, D. van Wees, A. Bastarrika, E. Chuvieco, G. R. van der Werf, African burned area and fire carbon emissions are strongly impacted by small fires undetected by coarse resolution satellite data. *Proc. Natl. Acad. Sci. U.S.A.* **118**, e2011160118 (2021).
56. T. C. Bond, R. W. Bergström, Light absorption by carbonaceous particles: An investigate review. *Aerosol Sci. Tech.* **40**, 27–67 (2006).
57. F. Peers, N. Bellouin, F. Waquet, F. Ducos, P. Goloub, J. Mollard, G. Myhre, R. B. Skeie, T. Takemura, D. Tanré, F. Thieuleux, K. Zhang, Comparison of aerosol optical properties above clouds between POLDER and AeroCom models over the South East Atlantic Ocean during the fire season. *Geophys. Res. Lett.* **43**, 3991–4000 (2016).
58. D. A. Lack, J. M. Langridge, R. Bahreini, C. D. Cappa, A. M. Middlebrook, J. P. Schwarz, Brown carbon and internal mixing in biomass burning particles. *Proc. Natl. Acad. Sci.* **109**, 14802–14807 (2012).
59. C. Denjean, J. Brito, Q. Libois, M. Mallet, T. Bourrianne, F. Burnet, A. Colomb, R. Dupuy, C. Flamant, P. Knippertz, A. Schwarzenboeck, Unexpected biomass burning aerosol absorption enhancement explained by black carbon mixing state. *Geophys. Res. Letters* **47**, e2020GL089055 (2020b).
60. H. Brown, X. Liu, Y. Feng, Y. Jiang, M. Wu, Z. Lu, C. Wu, S. Murphy, Radiative effect and climate impacts of brown carbon with the Community Atmosphere Model (CAM5). *Atmos. Chem. Phys.* **18**, 17745–17768 (2018).
61. A. Smirnov, B. N. Holben, D. M. Giles, I. Slutsker, N. T. O'Neill, T. F. Eck, A. Macke, P. Croot, Y. Courcoux, S. M. Sakerin, T. J. Smyth, T. Zielinski, G. Zibordi, J. I. Goes, M. J. Harvey, P. K. Quinn, N. B. Nelson, V. F. Radionov, C. M. Duarte, R. Losno, J. Sciare, K. J. Voss, S. Kinne, N. R. Nalli, E. Joseph, K. K. Moorthy, D. S. Covert, S. K. Gulev, G. Milinevsky, P. Larouche, S. Belanger, E. Horne, M. Chin, L. A. Remer, R. A. Kahn, J. S. Reid, M. Schulz, C. L. Heald, J. Zhang, K. Lapina, R. G. Kleidman, J. Griesfeller, B. J. Gaitley, Q. Tan, T. L. Diehl, Maritime aerosol network as a component of AERONET–first results and comparison with global aerosol models and satellite retrievals. *Atmos. Meas. Tech.* **4**, 583–597 (2011).
62. O. Dubovik, M. Herman, A. Holdak, T. Lapyonok, D. Tanré, J. L. Deuzé, F. Ducos, A. Sinyuk, A. Lopatin, Statistically optimized inversion algorithm for enhanced retrieval of aerosol properties from spectral multi-angle polarimetric satellite observations. *Atmos. Meas. Tech.* **4**, 975–1018 (2011).
63. O. Dubovik, T. Lapyonok, P. Litvinov, M. Herman, D. Fuertes, F. Ducos, A. Lopatin, A. Chaikovsky, B. Torres, Y. Derimian, X. Huang, M. Aspetsberger, C. Federspiel, *GRASP: A Versatile Algorithm for Characterizing the Atmosphere* (SPIE: Newsroom, 2014).
64. N. Schutgens, O. Dubovik, O. Hasekamp, O. Torres, H. Jethva, P. J. T. Leonard, P. Litvinov, J. Redemann, Y. Shinozuka, G. de Leeuw, S. Kinne, T. Popp, M. Schulz, P. Stier, AEROCOM and AEROSAT AAOD and SSA study – part 1: Evaluation and intercomparison of satellite measurements. *Atmos. Chem. Phys.* **21**, 6895–6917 (2021).
65. D. M. Winker, B. Hunt, M. J. McGill, Initial performance assessment of CALIOP. *Geophys. Res. Lett.* **34**, L19803 (2007).
66. N. G. Loeb, B. A. Wielicki, D. R. Doelling, G. L. Smith, D. F. Keyes, S. Kato, N. Manalo-Smith, T. Wong, Toward optimal closure of the Earth's top-of-atmosphere radiation budget. *J. Climate* **22**, 748–766 (2009).
67. L. Sogacheva, T. Popp, A. M. Sayer, O. Dubovik, M. J. Garay, A. Heckel, N. C. Hsu, H. Jethva, R. Kahn, P. Kolmonen, M. Kosmale, G. de Leeuw, R. C. Levy, P. Litvinov, A. Lyapustin, P. North, O. Torres, A. Arola, Merging regional and global aerosol optical depth records from major available satellite products. *Atmos. Chem. Phys* **20**, 2031–2056 (2020).

Acknowledgments: We thank the LASIC, AEROCLO-sA, ORACLES, and CLARIFY-2017 scientific community. We acknowledge all the principal investigators of the AERONET stations and their staff for establishing and maintaining the sites used in the present work. We acknowledge the World Climate Research Programme, which, through its Working Group on Coupled Modelling, coordinated and promoted CMIP6. We thank the climate modeling groups for producing and making available their model output, the ESGF for archiving the data and providing access, and the multiple funding agencies who support CMIP6 and ESGF. **Funding:** O.D. and C.C. acknowledge the support of CaPPA (Chemical and Physical Properties of the Atmosphere) project funded by ANR (ANR-ll-LABX-0005-01). J.M.H. was funded for the research under the NERC Large Grant NE/L013584/1 (CLARIFY-2017). M.Ma. is supported by the AErosols, RadiatiOn and CLOuds in southern Africa (AEROCLO-sA) project funded by the French National Research Agency under grant agreement no. ANR-15-CE01-0014-01, the French national programs LEFE/INSU and PNTS, the European Union's Seventh Framework Programme (FP7/2014-2018) under EUFAR2 contract no. 312609, and the South African National Research Foundation (NRF) under grant UID 105958. M.M. acknowledges the support of the French National Agency for Space Studies (CNES and AEROCLIM). B. J. was supported by the Met Office Hadley Centre Climate Programme funded by BEIS and Defra. **Author contributions:** M.Ma. and P.N. contributed to CMIP6 models evaluation, result analysis, and interpretation. B.J., M.Mi, J.M.H., C.C., and O.D. contributed to result interpretations. M.Ma. designed the study and wrote the manuscript. All authors contributed to manuscript improvement. **Competing interests:** O.D. supported GRASP SAS with scientific consulting and held actions of the company under "concours scientifique" convention of CNRS. The other authors declare that they have no competing interest. **Data and materials availability:** All data needed to evaluate the conclusions in the paper are present in the paper and/or the Supplementary Materials. The PARASOL/GRASP Models aerosol products are publicly available on the GRASP-OPNE website (https://grasp-open.com/products) and at the AERIS/ICARE Data and Services Center (https://www.icare.univ-lille.fr). The different AERONET data are available on the AERONET website (https://aeronet.gsfc.nasa.gov/).

Submitted 10 February 2021
Accepted 19 August 2021
Published 8 October 2021
10.1126/sciadv.abg9998

Citation: M. Mallet, P. Nabat, B. Johnson, M. Michou, J. M. Haywood, C. Chen, O. Dubovik, Climate models generally underrepresent the warming by Central Africa biomass-burning aerosols over the Southeast Atlantic. *Sci. Adv.* **7**, eabg9998 (2021).